NANO LETTERS

pubs.acs.org/NanoLett

Letter

Electron Irradiation Driven Nanohands for Sequential Origami

Chunhui Dai, Lianbi Li, Daniel Wratkowski, and Jeong-Hyun Cho*

Cite This: *Nano Lett.* 2020, 20, 4975−4984

Read Online

ACCESS | Metrics & More | Article Recommendations | Supporting Information

ABSTRACT: Sequence plays an important role in self-assembly of 3D complex structures, particularly for those with overlap, intersection, and asymmetry. However, it remains challenging to program the sequence of self-assembly, resulting in geometric and topological constrains. In this work, a nanoscale, programmable, self-assembly technique is reported, which uses electron irradiation as "hands" to manipulate the motion of nanostructures with the desired order. By assigning each single assembly step in a particular order, localized motion can be selectively triggered with perfect timing, making a component accurately integrate into the complex 3D structure without disturbing other parts of the assembly process. The features of localized motion, real-time monitoring, and surface patterning open the possibility for the further innovation of nanomachines, nanoscale test platforms, and advanced optical devices

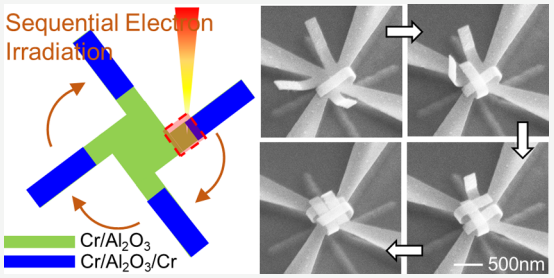

KEYWORDS: *sequential origami, weaving, electron irradiation, 3D, self-assembly, phase change*

Origami- and kirigami-inspired assembly of three-dimensional (3D) nanostructures has arisen to be a broad topic in the past two decades[1−23] due to its ability to alter physical properties of materials[5−13] and to use 3D space.[14−17] These 3D structures have been widely applied in metamaterial and plasmonic devices,[5,8,11,12,22,23] electronics,[1,6,14−17] and biomedical devices.[3,10,18−21] To realize 3D structures from two-dimensional (2D) nets, nanoscale folding and curving (spontaneous assembly) processes have been applied via a force generated by surface tension,[24−27] lattice mismatch,[7,14,19] and plastic deformation.[28−30] Though various 3D nanostructures have been demonstrated by tuning 2D nets,[31,32] it is still a great challenge to build complex 3D nanostructures with overlap, intersection, and asymmetry because one key factor of self-assembly is missing, namely programmable sequence. Sequence brings an additional dimension, time, to 3D self-assembly which allows better control of the interactions, such as moving pathway and relative positions, of structures in a complex, assembled 3D system. By assigning each single assembly step in an established order (i.e., a sequential, programmable self-assembly), localized motion can be selectively triggered with precise timing, making a component accurately integrate into a complex structure without disturbing other parts of the assembly processes. Several attempts to achieve sequential self-folding have been developed based on selective responsive material[33,34] or localized stimuli such as a microheater[35] or laser source.[36] However, the responsive material and stimuli used in these methods are restricted to large-scale,[33−36] and this size limitation makes it impossible to apply sequential self-assembly for the realization of complex 3D nanostructures.

Recently, ion-induced self-assembly processes attract great attention due to their ability for simultaneous localized stress generation and real-time monitoring,[26−29,37] where sequence is naturally encoded. However, the ion irradiation process suffers from two main limitations: material damage and limited directionality. First, all of the ion-induced assembly is based on the ion implantation process, which has evitable sputtering.[26−28] As a result of sputtering, incident ions bombard away the surface atoms, which cause severe physical damage on the sensitive material or ultrathin structures, resulting in limited universality and challenge for scale-down. Second, the ion beam based assembly techniques have dramatic restrictions on folding directionality. The current techniques can only achieve upward folding toward the incident ions. Moreover, because of the short ion implantation range (around tens of nanometers),[37] the folded components start to block the ion irradiation paths at the folding angle of 90°, impeding further folding. Thus, most of the assembled structures are limited to semi-3D such as the five face cubes.[26,27,37] The goal of nanoscale sequential assembly is to create intricate 3D nanostructures via precisely programing the timeline of each assembly steps. The physical damage and limited directionality bring critical challenges to fully explore the advantages of the ion beam for nanoscale sequential assembly. Therefore, a nanoscale sequential assembly technique that

Received: March 11, 2020
Revised: June 5, 2020
Published: June 5, 2020

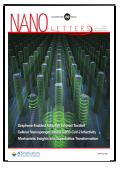

https://dx.doi.org/10.1021/acs.nanolett.0c01075
Nano Lett. 2020, 20, 4975−4984

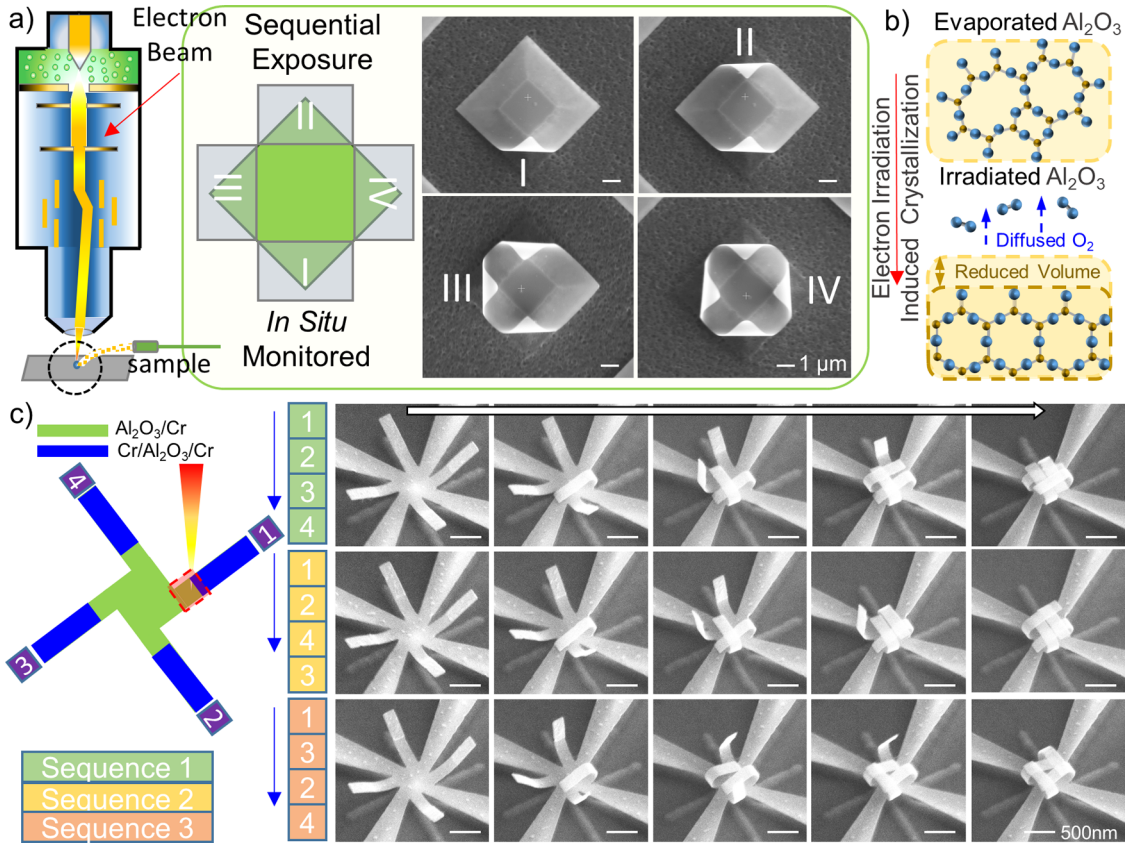

Figure 1. Conceptual schematics and SEM images showing the nanoweaving process triggered by electron irradiation induced crystallization. (a) Instrument setup of electron irradiation induced crystallization for programmable self-assembly. (b) Schematic showing the mechanism of electron induced crystallization. (c) Programmable weaving of nanoknots achieved by sequentially irradiating the thin films by electron beam. The four beams of the 2D pattern (labeled as "1", "2", "3", and "4") can be irradiated in different orders for sequential self-folding. Three different irradiation sequences have been demonstrated ("1234", "1243", and "1324"), resulting in different assembly outcomes.

allows the realization of sophisticated 3D structures remains absent.

Here we introduce a sequential, programmable self-assembly methodology that offers the capability to program the location, pattern, and energy of electron beam (e-beam) through the use of programmable e-beam scanning, thereby allowing control of the desired order for sequential self-assembly (Figure 1). This assembly approach also allows overlap, intersection, and asymmetry in assembly processes for building complex 3D nanostructures using the e-beam as a localized stimulus, which mimics origami and kirigami in nanoscale. Various complex 3D structures, specifically, a knot, latch, wrinkle, helix, butterfly, crane, and flower ring, are shown here as a proof of concept of sequential self-assembly in nanoscale.

To realize sequential self-assembly, we use an e-beam in a scanning electron microscope (SEM) as an energy source for triggering deformation of 2D patterns. The 2D bilayer (10 nm chromium, Cr/10 nm aluminum oxide, Al_2O_3) is formed on the silicon (Si) wafer through a standard electron beam lithography (EBL) process. Next, a reactive ion etching process is carried out to partially release the structures (Figure 1a,c). The detailed fabrication process is described in Supporting Information. An SEM offers nanoscale, localized e-beam irradiation with precisely controllable beam-position and real-time images showing the current status of assembly, leading to an *in situ* monitored self-assembly process (Figure 1a).[26−30,38−40] The combination of programmable e-beam irradiation and real-time imaging capability in an SEM mimics the functions of "hands" and "eyes" of a human being for doing paper origami, which significantly enhances the controllability of assembly. Stress is induced in released bilayers as a result of volume changes in the Al_2O_3 layer caused by outgassing and atom rearrangement during crystallization when localized heat generated by the e-beam irradiation is applied (Figure 1b). The stress induced on the specific area deforms the freestanding thin films. As localized stimuli are applied to targeted areas with a desired order, sequential self-assembly is achieved while being simultaneously monitored (Figure 1a). As a proof of concept, three different e-beam sequences are demonstrated constituting programmable nanoweaving processes that involve high time and space complexity (Figure 1c, and SI Video 1 and Video 2). By tuning the weaving sequence, four knots with different internal spatial relations are demonstrated.

The driving force of assembly is the localized stress generated by electron irradiation-induced volume shrinkage of Al_2O_3 films. This volume change is caused by the phase change (crystallization) of e-beam evaporated Al_2O_3 films, which is associated with extra oxygen outgassing and atomic rearrangement. To confirm the mechanism, transmission electron microscopy (TEM) and atomic force microscopy (AFM) are used to analyze the interaction between electron irradiation and evaporated Al_2O_3 films. First, TEM characterization is carried out on a partially curved tubular structure (3 nm Cr and 30 nm Al_2O_3) for studying the phase change of Al_2O_3 (Figure 2a). A thick Al_2O_3 layer (30 nm) is used so that both the initial amorphous state and the crystallized state can be directly

https://dx.doi.org/10.1021/acs.nanolett.0c01075
Nano Lett. 2020, 20, 4975−4984

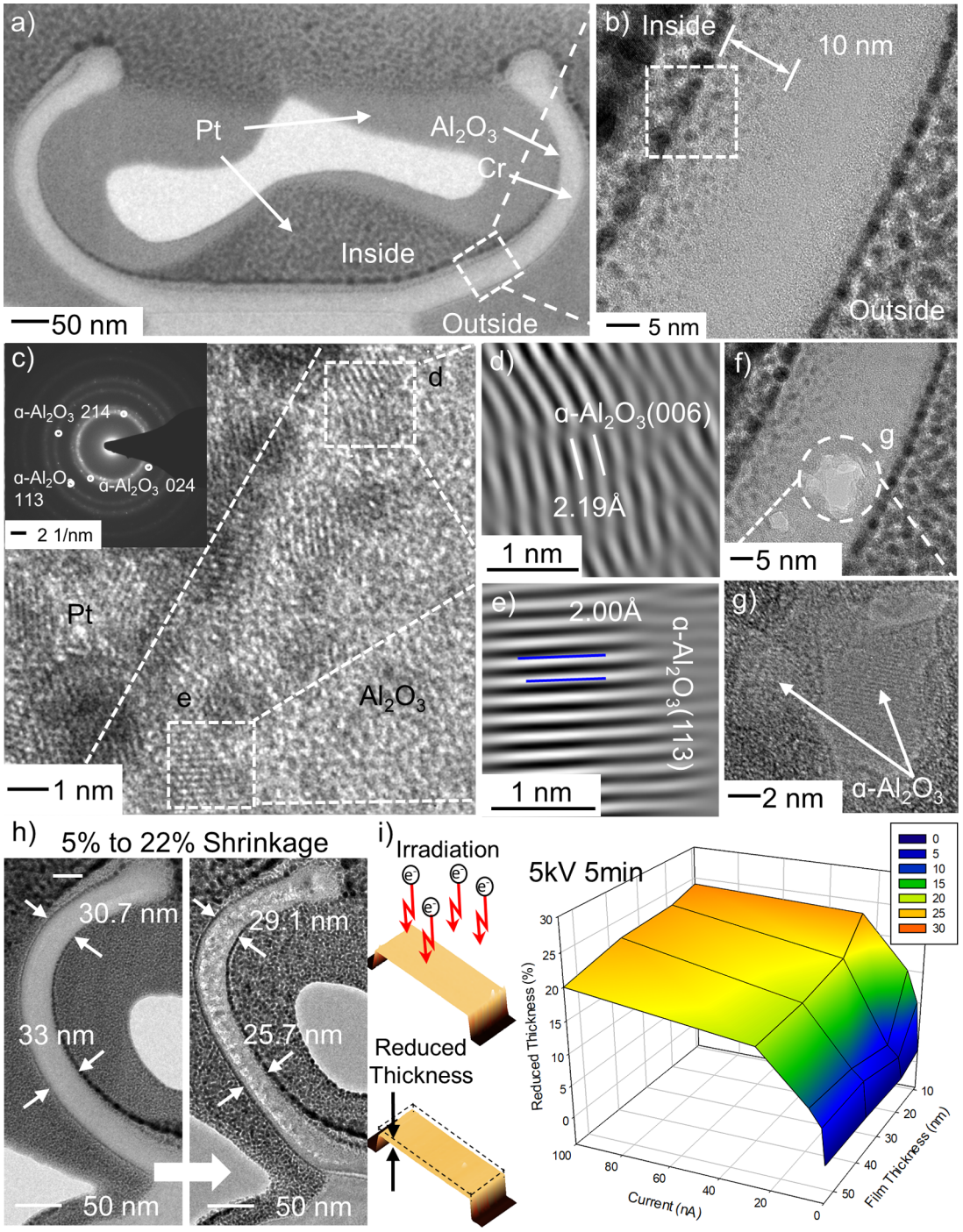

Figure 2. TEM and AFM analyses of the electron irradiation induced material change. (a) TEM sample of a partially curved tube structures prepared by FIB. (b) TEM image of the analyzed area of the tube structures. (c) HRTEM image of the surface of the tube structure, indicating the electron irradiation induced Al_2O_3 nanocrystals. The inset is the selected area electron diffraction (SAED) analysis of the partially curved tube, which shows the amorphous Al_2O_3 are mostly crystallized into α-Al_2O_3 with different orientations including [213], [113], [024] and so on. (d,e) Fourier transformation analysis of the nucleated Al_2O_3 area. Clear crystal structures with interplanar d-spacing of (d) 0.219 nm and (e) 0,200 nm are overserved, which are corresponding to the orientation of [006] and [113], respectively. (f,g) High energy electron irradiation triggered crystallization in TEM. (h) TEM induced in situ volume change of the tube left arm due to crystallization. (i) AFM measurement for Al_2O_3 volume change under electron irradiation (5 kV) with different beam currents and film thicknesses for 5 min.

observed and compared within the thin film. The partially curved tube is embedded in platinum (Pt) and then cut out from the original sample using ion milling to get cross-sectional TEM images. The detailed sample preparation and characterization are described in Supporting Information (Figure S1). An energy dispersive spectroscopy (EDS) mapping is used to identify the composition of the bilayers (Figure S2), which clearly shows the distribution of Al_2O_3 and Cr. The pristine condition of the Al_2O_3 layer before self-curving (e-beam radiation) is amorphous; however, in the curved regime of the Al_2O_3 tube after self-curving the contrast representing crystallization of Al_2O_3 varies significantly near the inside, especially from the surface to the

https://dx.doi.org/10.1021/acs.nanolett.0c01075
Nano Lett. 2020, 20, 4975−4984

depth of 10 nm (Figure 2b). This demonstrates that the nanocrystallites (NCs) nucleate, grow in the near-surface regions of the Al_2O_3, and propagate into the amorphous Al_2O_3 layer while under e-beam exposure. The nanocrystallites are also confirmed by selected area electron diffraction (SAED) of the curved tube outlined in the dashed square in Figure 2a (Figure 2c inset). The high-resolution TEM image (Figure 2c) and its fast Fourier transform analysis (Figure 2d,e) show irradiation results in crystallization of the amorphous-Al_2O_3 matrix. Most of the amorphous-Al_2O_3 are crystallized into α-Al_2O_3 in which randomly oriented nanocrystallites (α-Al_2O_3) are formed, including [113], [024], [214], and [006] (Figure 2c–e). The Fourier transform analysis of two nanocrystallites in Figure 2c shows clear crystal structures with interplanar *d*-spacing of 0.219 nm (Figure 2d, orientation, [006]) and 0.200 nm (Figure 2e, orientation, [113]). To confirm e-beam triggered crystallization, the amorphous-Al_2O_3 region is irradiated by a high voltage e-beam (300 kV) for 10 s, which provides continuous driving force to form the nanocrystallites. As a result, the central area of approximately 10 nm in diameter is completely transformed from amorphous-Al_2O_3 to α-Al_2O_3 (Figure 2f,g). According to the interplanar *d*-spacing of 0.238 and 0.255 nm (Figure S3), the orientation of α-Al_2O_3 nanocrystallites are confirmed as [110] and [104], respectively. This observation shows clear evidence that electron irradiation has the ability to trigger a crystallization process in amorphous materials. As for the mechanism of electron irradiation induced crystallization, it still remains greatly controversial. Previous studies suggested high temperature induced by e-beam irradiation is the key factor for crystallization of the amorphous thin film.[41] However, Nakamura et al. later found that the temperature rise caused by e-beam heating is much lower than the required annealing temperature for Al_2O_3 crystallization.[42] Thus, the electronic excitation process, rather than e-beam heating-induced temperature raise, is the dominant factor for the migration of atoms in the materials, triggering crystallization. On the basis of this theory, electron irradiation even at low acceleration voltages and currents (5 kV, 0.8 nA) directly break and rearrange thermodynamically unstable bonds in the amorphous material, resulting in crystallization without the assistance of temperature rise. The crystallization induces volume shrinkage and, in our case, 5% to 22% thickness changes have been observed after e-beam irradiation in a TEM, which results in further structural deformation even if the tube is embedded in a Pt coating (Figure 2h). The variation is because of the different initial and final crystallization status. The curved tube is already slightly crystallized during self-assembly. Also, the irradiation dose and positions exposed to the electron beam in the TEM for imaging is not well controlled so that the shrinkage is not uniform along the thin film. However, this observation provides a direct evidence that irradiation induced crystallization could cause significant volume change of Al_2O_3. Further, the e-beam induced volume change is systematically investigated on irradiated amorphous Al_2O_3 plateaus (6 μm × 6 μm). Even though different combinations of plateau thickness (9, 18, 36, and 54 nm) and e-beam current (1.6, 6.4, 26, and 100 nA) are applied, the measured AFM results of thickness reduction show saturation at around 22% among all the samples (Figure 2i), which indicates the crystallization is completed at this stage and confirms the observation in TEM. The detailed experiment setup and data analysis of this measurement is provided in the Supporting Information.

Numerical analysis for achieving a quantitative understanding of curving behavior is conducted by studying the effects of film thickness and coverage length of the bilayer system. Two sets of experiments are carried out on the bilayer beams with 100 nm width and 1 μm length. First, the thickness of the Cr layer is fixed at 10 nm and the thickness of Al_2O_3 is varied to four different quantities, 10, 20, 30, and 40 nm (Figure 3a–d). Then, the thickness of the Al_2O_3 layer is fixed and the thickness of the Cr is

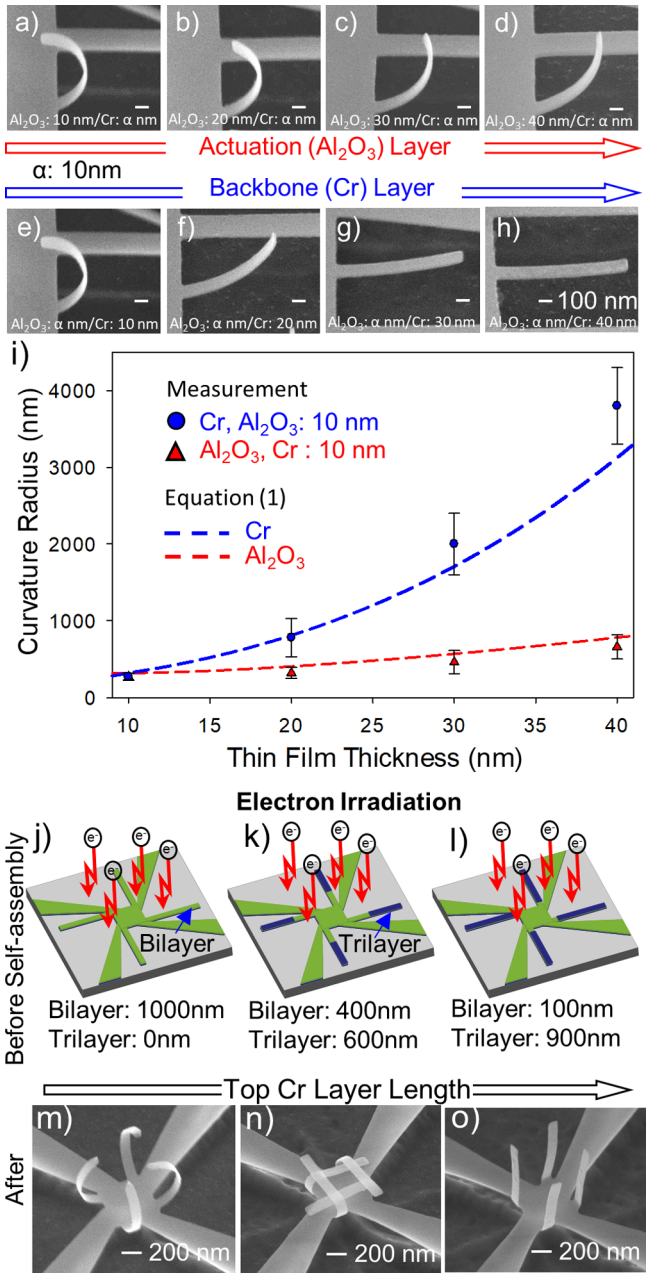

Figure 3. Effect of film thickness and relative coverage on self-assembly. The self-assembly result of the samples with (a–d) 10 nm Cr and increasing Al_2O_3 layer thickness (10, 20, 30, and 40 nm) and (e–h) 10 nm Al_2O_3 and increasing Cr layer thickness (10, 20, 30, and 40 nm). (i) The curving radius of the different combinations of material thickness are measured and modeled. (j–l) The schematic and (m-o) SEM images showing the effect of relative coverage of the additional Cr layer on the assembly behavior of the Cr/Al_2O_3 bilayer system. (j,m) The curving behavior of 1 μm long beams is transformed into (k,n) weaving and (l,o) folding with 600 and 900 nm of additional Cr layer coverage.

https://dx.doi.org/10.1021/acs.nanolett.0c01075
Nano Lett. 2020, 20, 4975–4984

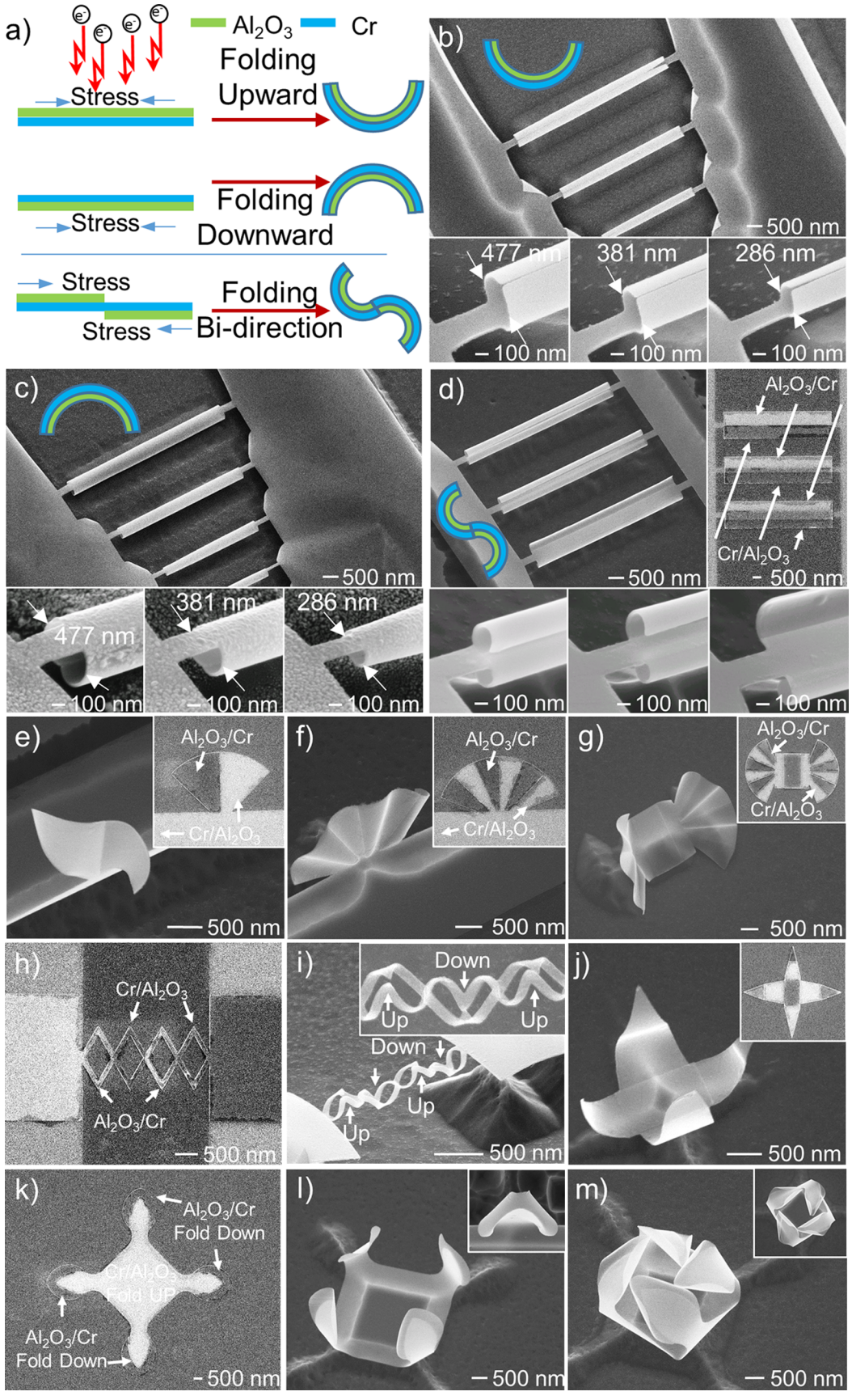

Figure 4. Multidirectional assembly of 3D complex nanostructures. (a) Schematics and (b–d) SEM images showing the bidirectional curving of tube structures. Various sizes of the tube structures are realized with (b) upward, (c) downward, and (d) combined directional curving. (e–m) Multidirectional assembly of complex nanoarchitectures.

https://dx.doi.org/10.1021/acs.nanolett.0c01075
Nano Lett. 2020, 20, 4975–4984

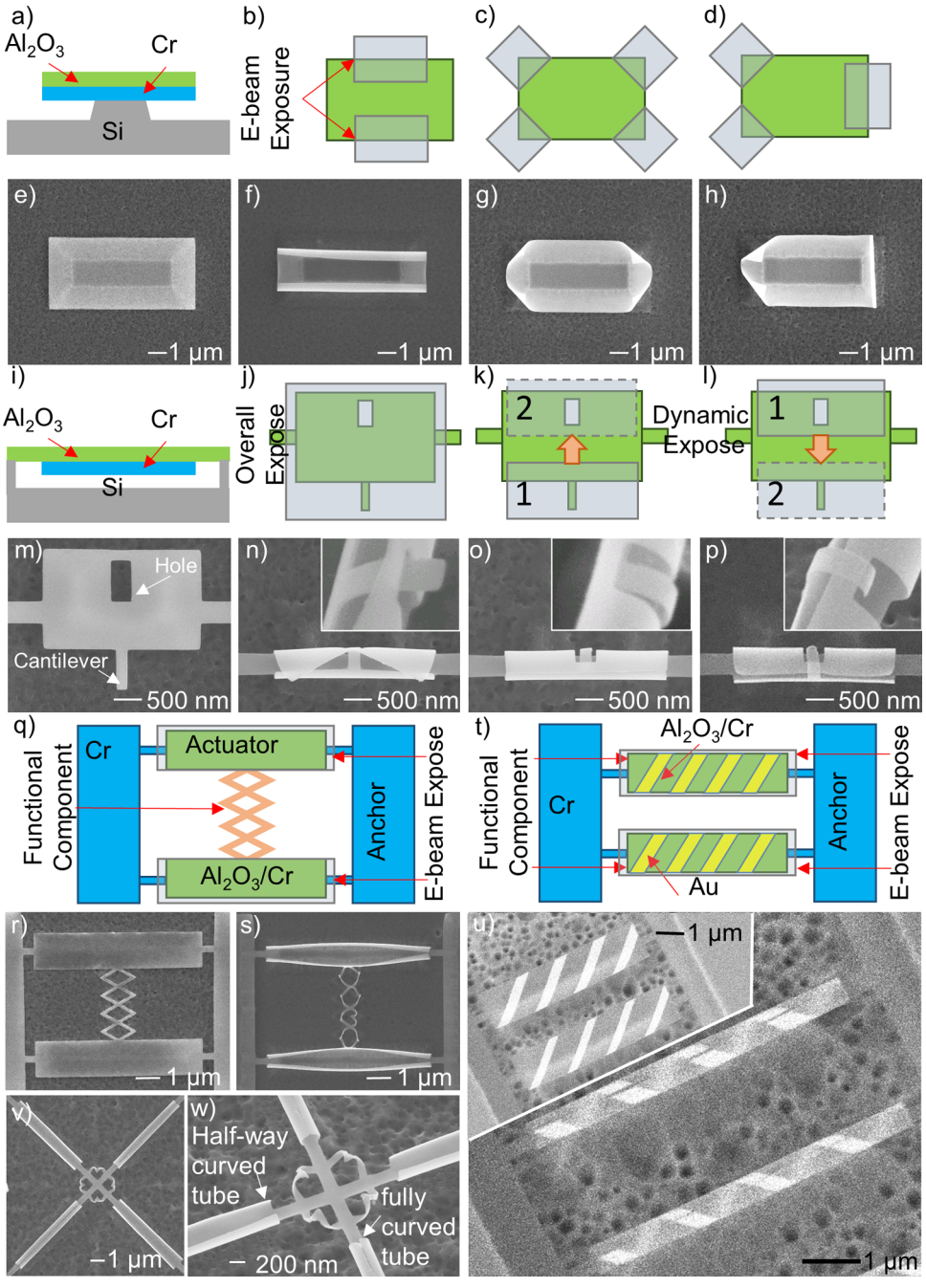

Figure 5. Schematic and SEM images showing the programmable assembly and potential applications realized by e-beam induced self-assembly. (a–h) Different assembly outcomes are achieved on a rectangular sheet with (b,f) curved edges, (c,g) curved corners, or (d,h) combination of both behaviors via localized irradiation. (i–p) The programmed irradiation triggers (k,o) internal and (l,p) external locking behaviors. (q–s) Nano-stresstest platform and (t,u) nanochiral materials have been realized via integrating functional components with the curving structures. (v,w) A system integrated with various structures and assembly behavior is achieved.

changed in the same manner as for Al_2O_3 in the first case (Figure 3e–h). The e-beam voltage, current, exposure time, and magnification are set to be 5 kV, 6.4 nA, 100 s, and 5000× to maintain an identical irradiation condition. Increasing the deposited thickness of the passive curving layer (Cr) shows a more critical influence on changes to the radius curvature than increasing the initial thickness of the active curving layer (Al_2O_3) (Figure 3a–i) even though there is no significant discrepancy between the Young's modulus of Cr and Al_2O_3. This behavior is attributed to increased Cr thickness inducing additional resistance to bending. Because of the enhanced constraints, the out-of-plane strain becomes more dominant and the in-plain strain is significantly reduced, leading to a larger curving radius. In the case of varying the Al_2O_3 layer, the increased Al_2O_3 thickness causes higher resistance but also more stress generation when acting as the actuation (active) layer for curving, resulting in a smaller radius of curvature when compared to the cases of increased Cr thickness. On the basis of this mechanism, a new model (eq 1) inspired by thermal expansion curving of thin films[43] has been developed. In the model, the radius of curvature, R, is described as

https://dx.doi.org/10.1021/acs.nanolett.0c01075
Nano Lett. 2020, 20, 4975–4984

$$R = h^2 \frac{3\cdot(1+m)^2 + (1+m\cdot n)\left[m^2 + \frac{1}{m\cdot n}\right]}{6\cdot Q_a \cdot E \cdot T_a \cdot (1+m)^2} \quad (1)$$

where T_a is the thickness of Al_2O_3 film, T_c is the thickness of Cr film, $h = T_a + T_c$ is the thickness of bilayer system, $m = T_a/T_c$ is the thickness ratio of the Al_2O_3 layer to the Cr layer, $n = Y_a/Y_c$ is the ratio of the Young's modulus of Al_2O_3 to that of Cr, and E stands for e-beam irradiation energy. $Q_a = 15.6/J$ is the shrink coefficient obtained by curve fitting. The detailed derivation of the equation is shown in Supporting Information and Figure S6. As plotted in Figure 3i, the theoretical modeling result coincides with the experimental measurement, which shows the radius depends not only on the overall bilayer thickness but also on the thickness ratio of the two materials. This model offers an insight into the mechanism of electron irradiation triggered assembly and assists with structural design.

In addition, the curving behavior can be further modified via arranging the material layout and structural configuration. Under electron irradiation, the deformation is uniform along the bilayer (10 nm Cr/10 nm Al_2O_3) cantilever (Figure 3j,m). Though slight curving variation exists due to the different energy absorption between upper and lower parts, the curving cantilever is relatively isotropic in 3D. By applying a third Cr layer on top of the bilayer system, the curving behavior (Figure 3j,m) is confined to the bilayer-only areas (Figure 3k,l,n,o). The different coverages of the trilayer area can lead to different assembly outcomes: weaving (Figure 3k,n) and folding (Figure 3l,o). The detailed information for controlling the assembly outcomes is described in the Supporting Information.

The e-beam triggered self-assembly process is not limited to unidirectional curving or folding. By modifying the material layout, the area generating stress in the thin film can be engineered. If the relative positions of the Cr (10 nm) and Al_2O_3 (10 nm) are flipped, the stress will be induced in the bottom layer instead of the top layer, transforming the upward curving into downward curving (Figure 4a). Both the upward (Figure 4b) and downward (Figure 4c) curved tubes with different diameters (477, 381, and 286 nm) are realized by tuning the material layout. When two different material layouts are cemented next to each other, both upward and downward curving are achieved in the same structure thereby forming bidirectional curving (Figure 4a). On the basis of the design of the conjunct area, bidirectional curved tubes with different radii have been realized (Figure 4d). The 5 keV electrons have implantation ranges of around 100 and 400 nm in Cr and Al_2O_3, respectively (Figures S4 and S7). Thus, the electrons can easily pass through the 10 nm Cr or 10 nm Al_2O_3 film. Even though the energy absorption will be higher for the top layers, the 10 nm thick thin film is too thin to induce significant changes, resulting in similar curvature (Figure 4d). With more degrees of freedom, multidirectional assembly can be achieved. By cementing together three different material layouts (Figure 4e inset), curving structures with three distinct curving directions have been assembled with an upward curving base area and bidirectionally folding sector structures (Figure 4e). By integrating more sections of different layouts in the same pattern of Figure 4e, an oriental fan is demonstrated on the Si substrate (Figure 4f). To further demonstrate the capabilities of this approach, simplified butterfly, chain, and crane shapes have been assembled based on the same strategy (Figure 4g–j). This powerful nanoscale self-assembly process enables various functions human hands can do such as folding, curving, stretching, and weaving, showing the possibility to fully mimic origami and kirigami. As a demonstration, a flower ring, which consists of various folding or curving sections, has been assembled by precisely controlling the irradiation area, location, and sequence (Figure 4k–m). The videos for each of the folding behaviors shown in Figure 4 are provided in SI Video 3, Video 4, Video 5, Video 6, and Video 7.

This e-beam-induced, sequential, programmable self-assembly methodology opens up various application possibilities due to precise control of the irradiation pattern, sequence, and energy exposed to the nanostructures. The combined functions of controllable, localized irradiation, and real-time imaging make it possible to trigger localized folding or curving. Through modifying the irradiation pattern on a released bilayer system (10 nm Cr and 10 nm Al_2O_3) (Figure 5a,e), a rectangular film has been assembled into three completely different forms with two curved edges (Figure 5b,f), four curved corners (Figure 5c,g), and a combination of a curved edge and corners (Figure 5d,h, and SI Video 8). The diverse outcomes achieved from the same starting 2D structures demonstrate the ability to overcome the geometric limits of 2D patterns. Asymmetric geometries can be easily achieved by sequentially assigning different localized assembly behaviors on a structure (Figure 5d,h). It should be noted that the direction of induced strain can hardly be changed by additional irradiation because of area moment of inertia induced by the initial deformation.[44] For example, the left part of Figure 5h cannot be modified to match the right part via further electron irradiation. This means that sequence also plays an important role in controlling the transformation strain in the thin film. In addition, this assembly technique shows the possibility to realize mechanical functions by modifying the motion of thin films. A suspended bilayer system (10 nm Cr and 10 nm Al_2O_3) with a hole and a cantilever is defined on a Si substrate to demonstrate a locking behavior (Figure 5i,m). When the overall structure is exposed to electron irradiation, universal stress is induced in the thin films. As a result, the cantilever and corners fold up prior to the rest of the structure, which results in these portions contacting the main portion of the structure prematurely thereby impeding further folding (Figure 5j,n and SI Video 9). When the irradiation area is well programmed to move from the cantilever to the hole (irradiate pattern 1 first and then move to pattern 2 in Figure 5k), the cantilever is designated to fold before the area around the hole. This irradiation sequence produces a tube structure with the cantilever penetrated through the hole as an internal locking mechanism (Figure 5o and SI Video 10). If the irradiation sequence is reversed (Figure 5l), the beam hooks through the hole from the outside of the tube, locking externally (Figure 5p and SI Video 11). It should be noted this sequential, programmable assembly process enables tunable outcomes for the realization of various 3D nanostructures functionalized for specific purposes even though the 2D patterns are the same before self-assembly. The desired sequence of irradiation brings an additional dimension into 3D structure design, allowing a researcher to further modify the 3D architecture after 2D pattern design.

The movement of the thin film induced by localized e-beam irradiation can be further used as a single turn actuator to power a nanoscale test platform. A nanoscale stress test platform that consists of anchors, two tubular actuators, and a nanospring (10 nm Cr and 10 nm Al_2O_3) as a functional component has been fabricated (Figure 5q–s). While electron irradiation is delivered to the actuator patterns, the patterns curl up to be tubular

https://dx.doi.org/10.1021/acs.nanolett.0c01075
Nano Lett. 2020, 20, 4975−4984

structures and stretch the 2D nets which become a tensioned nanospring (Figure 5s and SI Video 12). With further design and calibration, this test platform may be applied to nanoscale stress tests for various applications such as flexible material or kirigami structures. The Cr/Al_2O_3 bilayer can only achieve one time deformation and thus not be able to achieve the reversible assembly process and actuation behavior demonstrated in microscale graphene bimorphs[45] and cross-linkable polymer trilayers[46] yet. However, with further exploration of electron irradiation interaction with phase change materials, a real actuator should able to be demonstrated based on irradiation induced reversible material phase change, leading to the innovation of nanomachines. In addition, surface patterning with secondary materials can be incorporated into the 3D structures to achieve advanced 3D functional nanomaterials and devices. As a proof of concept, chiral structures have been realized inside a nanotube by integrating patterns (gold stripes) on top of a 10 nm Al_2O_3 rectangular thin film (before e-beam irradiation, Figure 5t and inset in Figure 5u; after e-beam irradiation, Figure 5u, SI Video 13). Moreover, because of the localized stress generation with the desired energy supplied at each location, assembly processes with various functionalities can be integrated next to each other, showing the potential to build comprehensive devices. This ability is demonstrated with the creation of a flower shape (lucky clover) and tubes with different radii of curvature all on the same substrate (Figure 4v,w).

In conclusion, a sequential, programmable self-assembly methodology triggered by electron irradiation is developed. By combining the design of 2D patterns, application of localized stress generation, and execution of 3D assembly steps in a particular, desired order, it is possible to achieve various functions of human hands including multidirectional folding, curving, stretching, weaving, and sequential assembling, thereby enabling origami and kirigami to be mimicked on the nanoscale level to allow the realization of tunable 3D structures. Various complex 3D nanostructures and prototype devices are demonstrated based on this method, showing the possibilities for pushing self-assembly to a new level for applications in nanoscale 3D devices, machines, and robotics. Moreover, the compatibility with electron beam makes it possible to equip this technique with advanced functions of existing ebeam tools and lead to the further development.

■ ASSOCIATED CONTENT

Supporting Information

The Supporting Information is available free of charge at https://pubs.acs.org/doi/10.1021/acs.nanolett.0c01075.

Video 1: Sequential programmable folding of the four corners of a square bilayer sheet (MP4)

Video 2: Nanoweaving achieved via sequential programmable folding (MP4)

Video 3: Multidirectional folding for assembly of bidirectionally curved tubes (MP4)

Video 4: Multidirectional folding for three-dimensional assembly (MP4)

Video 5: Multidirectional folding for assembly of a 3D chain (MP4)

Video 6: Multidirectional folding for assembly of a crane (MP4)

Video 7: Multidirectional folding for assembly of a flower ring (MP4)

Video 8: Sequential programmable folding for integrating different folding outcomes in a rectangular bilayer sheet (MP4)

Video 9: Locking behavior achieved without the control of irradiation sequence and location (MP4)

Video 10: Internal locking achieved via precise control of irradiation sequence and location (MP4)

Video 11: External locking achieved via precise control of irradiation sequence and location (MP4)

Video 12: Stretching test platform demonstrated by two tubular single turn actuators and a stretchable nanospring (MP4)

Video 13: Self-assembled nanotube with functional surface patterns (MP4)

Fabrication of 2D structures; TEM sample preparation and analysis; AFM measurement of irradiation induced volume change in amorphous Al_2O_3 plateaus; simulation of electron irradiation in Al_2O_3; characterization of the chemical composition and volume change of irradiated Al_2O_3 films; modeling of shrinkage induced assembly of a bilayer system; controlling assembly outcomes using a $Cr/Al_2O_3/Cr$ trilayer; simulation of electron irradiation in Cr (PDF)

■ AUTHOR INFORMATION

Corresponding Author

Jeong-Hyun Cho − *Department of Electrical and Computer Engineering, University of Minnesota, Minneapolis, Minnesota 55455, United States;* orcid.org/0000-0003-2870-1960; Email: jcho@umn.edu

Authors

Chunhui Dai − *Department of Electrical and Computer Engineering, University of Minnesota, Minneapolis, Minnesota 55455, United States*

Lianbi Li − *Department of Electrical and Computer Engineering, University of Minnesota, Minneapolis, Minnesota 55455, United States; School of Science, Xi'an Polytechnic University, Xi'an 710000, People's Republic of China*

Daniel Wratkowski − *Department of Electrical and Computer Engineering, University of Minnesota, Minneapolis, Minnesota 55455, United States*

Complete contact information is available at: https://pubs.acs.org/10.1021/acs.nanolett.0c01075

Author Contributions

J.H.C. conceived and supervised the research. C.D. designed and fabricated the sample, built the model, and analyzed the data. L.L. assisted the TEM data analysis. D.W. assisted the sample fabrication. All authors contributed to writing the manuscript.

Funding

NSF CAREER Award (CMMI-1454293).

Notes

The authors declare no competing financial interest.

■ ACKNOWLEDGMENTS

This material is based upon work supported by an NSF CAREER Award (CMMI-1454293). This work was supported partially by the National Science Foundation through the University of Minnesota MRSEC under Award Number DMR-1420013. Parts of this work were carried out in the Characterization Facility, University of Minnesota, a member of the NSF-

funded Materials Research Facilities Network (www.mrfn.org) via the MRSEC program. Portions of this work were conducted in the Minnesota Nano Center, which is supported by the National Science Foundation through the National Nano Coordinated Infrastructure Network, Award Number NNCI1542202. C.D. acknowledges support from the Doctoral Dissertation Fellowship from University of Minnesota. The authors would like to thank Dr. Jason Myers for providing valuable support on TEM measurement.

REFERENCES

(1) Gracias, D. H.; Tien, J.; Breen, T. L.; Hsu, C.; Whitesides, G. M. Forming electrical networks in three dimensions by self-assembly. *Science* **2000**, *289*, 1170−1172.
(2) Blees, M. K.; Barnard, A. W.; Rose, P. A.; Roberts, S. P.; McGill, K. L.; Huang, P. Y.; Ruyack, A. R.; Kevek, J. W.; Kobrin, B.; Muller, D. A.; McEuen, P. L. Graphene kirigami. *Nature* **2015**, *524*, 204.
(3) Gladman, A. S.; Matsumoto, E. A.; Nuzzo, R. G.; Mahadevan, L.; Lewis, J. A. Biomimetic 4D printing. *Nat. Mater.* **2016**, *15*, 413.
(4) Cho, J.; Gracias, D. H. Self-assembly of lithographically patterned nanoparticles. *Nano Lett.* **2009**, *9*, 4049−4052.
(5) Tang, Y.; Lin, G.; Yang, S.; Yi, Y. K.; Kamien, R. D.; Yin, J. Programmable kiri-kirigami metamaterials. *Adv. Mater.* **2017**, *29*, 1604262.
(6) Shyu, T. C.; Damasceno, P. F.; Dodd, P. M.; Lamoureux, A.; Xu, M.; Shlian, M.; Shtein, M.; Glotzer, S. C.; Kotov, N. A. A kirigami approach to engineering elasticity in nanocomposites through patterned defects. *Nat. Mater.* **2015**, *14*, 785.
(7) Tian, Z.; Xu, B.; Hsu, B.; Stan, L.; Yang, Z.; Mei, Y. Reconfigurable vanadium dioxide nanomembranes and microtubes with controllable phase transition temperatures. *Nano Lett.* **2018**, *18*, 3017−3023.
(8) Wang, X.; Dong, K.; Choe, H. S.; Liu, H.; Lou, S.; Tom, K. B.; Bechtel, H. A.; You, Z.; Wu, J.; Yao, J. Multifunctional microelectro-opto-mechanical platform based on phase-transition materials. *Nano Lett.* **2018**, *18*, 1637−1643.
(9) Xu, B.; Tian, Z.; Wang, J.; Han, H.; Lee, T.; Mei, Y. Stimuli-responsive and on-chip nanomembrane micro-rolls for enhanced macroscopic visual hydrogen detection. *Sci. Adv.* **2018**, *4*, No. eaap8203.
(10) Xu, W.; Qin, Z.; Chen, C.T.; Kwag, H. R.; Ma, Q.; Sarkar, A.; Buehler, M. J.; Gracias, D. H. Ultrathin thermoresponsive self-folding 3D graphene. *Sci. Adv.* **2017**, *3*, No. e1701084.
(11) Agarwal, K.; Liu, C.; Joung, D.; Park, H.-R.; Jeong, J.; Kim, D.-S.; Cho, J.-H. Three-dimensionally coupled THz octagrams as isotropic metamaterials. *ACS Photonics* **2017**, *4*, 2436−2445.
(12) Joung, D.; Nemilentsau, A.; Agarwal, K.; Dai, C.; Liu, C.; Su, Q.; Li, J.; Low, T.; Koester, S. J.; Cho, J.-H. Self-assembled three-dimensional graphene-based polyhedrons inducing volumetric light confinement. *Nano Lett.* **2017**, *17*, 1987−1994.
(13) Joung, D.; Gu, T.; Cho, J. Tunable optical transparency in self-assembled three-dimensional polyhedral graphene oxide. *ACS Nano* **2016**, *10*, 9586−9594.
(14) Grimm, D.; Bof Bufon, C. C.; Deneke, C.; Atkinson, P.; Thurmer, D. J.; Schäffel, F.; Gorantla, S.; Bachmatiuk, A.; Schmidt, O. G. Rolled-up nanomembranes as compact 3D architectures for field effect transistors and fluidic sensing applications. *Nano Lett.* **2013**, *13*, 213−218.
(15) Karnaushenko, D.; Karnaushenko, D. D.; Makarov, D.; Baunack, S.; Schäfer, R.; Schmidt, O. G. Self-assembled on-chip-integrated giant magneto-impedance sensorics. *Adv. Mater.* **2015**, *27*, 6582−6589.
(16) Huang, W.; Zhou, J.; Froeter, P. J.; Walsh, K.; Liu, S.; Kraman, M. D.; Li, M.; Michaels, J. A.; Sievers, D. J.; Gong, S.; Li, X. Three-dimensional radio-frequency transformers based on a self-rolled-up membrane platform. *Nat. Electron.* **2018**, *1*, 305.
(17) Torikai, K.; Furlan de Oliveira, R.; Starnini de Camargo, D. H.; Bof Bufon, C. C. Low-voltage, flexible, and self-encapsulated ultra-compact organic thin-film transistors based on nanomembranes. *Nano Lett.* **2018**, *18*, 5552−5561.
(18) Magdanz, V.; Medina-Sánchez, M.; Schwarz, L.; Xu, H.; Elgeti, J.; Schmidt, O. G. Spermatozoa as functional components of robotic microswimmers. *Adv. Mater.* **2017**, *29*, 1606301.
(19) Magdanz, V.; Guix, M.; Hebenstreit, F.; Schmidt, O. G. Dynamic polymeric microtubes for the remote-controlled capture, guidance, and release of sperm cells. *Adv. Mater.* **2016**, *28*, 4084−4089.
(20) Malachowski, K.; Breger, J.; Kwag, H. R.; Wang, M. O.; Fisher, J. P.; Selaru, F. M.; Gracias, D. H. Stimuli-responsive theragrippers for chemomechanical controlled release. *Angew. Chem., Int. Ed.* **2014**, *53*, 8045−8049.
(21) Leong, T. G.; Randall, C. L.; Benson, B. R.; Bassik, N.; Stern, G. M.; Gracias, D. H. Tetherless thermobiochemically actuated microgrippers. *Proc. Natl. Acad. Sci. U. S. A.* **2009**, *106*, 703−708.
(22) Joung, D.; Agarwal, K.; Park, H.-R.; Liu, C.; Oh, S.-H.; Cho, J.-H. Self-assembled multifunctional 3D microdevices. *Adv. Electron. Mater.* **2016**, *2*, 1500459.
(23) Cho, J.; Keung, M. D.; Verellen, N.; Lagae, L.; Moshchalkov, V. V.; Van Dorpe, P.; Gracias, D. H. Nanoscale origami for 3D optics. *Small* **2011**, *7*, 1943−1948.
(24) Dai, C.; Joung, D.; Cho, J. Plasma triggered grain coalescence for self-assembly of 3D nanostructures. *Nano-Micro Lett.* **2017**, *9*, 27.
(25) Cho, J.; James, T.; Gracias, D. H. Curving nanostructures using extrinsic stress. *Adv. Mater.* **2010**, *22*, 2320−2324.
(26) Dai, C.; Cho, J. In situ monitored self-assembly of three-dimensional polyhedral nanostructures. *Nano Lett.* **2016**, *16*, 3655−3660.
(27) Dai, C.; Agarwal, K.; Cho, J. Ion-induced localized nanoscale polymer reflow for three-dimensional self-assembly. *ACS Nano* **2018**, *12*, 10251−10261.
(28) Chalapat, K.; Chekurov, N.; Jiang, H.; Li, J.; Parviz, B.; Paraoanu, G. S. Self-organized origami structures via ion-induced plastic strain. *Adv. Mater.* **2013**, *25*, 91−95.
(29) Wu, C.; Li, F.; Pao, C.; Srolovitz, D. J. Folding sheets with ion beams. *Nano Lett.* **2017**, *17*, 249−254.
(30) Mao, Y.; Zheng, Y.; Li, C.; Guo, L.; Pan, Y.; Zhu, R.; Xu, J.; Zhang, W.; Wu, W. Programmable bidirectional folding of metallic thin films for 3D chiral optical antennas. *Adv. Mater.* **2017**, *29*, 1606482.
(31) Tian, Z.; Huang, W.; Xu, B.; Li, X.; Mei, Y. Anisotropic rolling and controlled chirality of nanocrystalline diamond nanomembranes toward biomimetic helical frameworks. *Nano Lett.* **2018**, *18*, 3688−3694.
(32) Abdullah, A. M.; Li, X.; Braun, P. V.; Rogers, J. A.; Hsia, K. J. Self-folded gripper-like architectures from stimuli-responsive bilayers. *Adv. Mater.* **2018**, *30*, 1801669.
(33) Mao, Y.; Yu, K.; Isakov, M. S.; Wu, J.; Dunn, M. L.; Jerry Qi, H. Sequential self-folding structures by 3D printed digital shape memory polymers. *Sci. Rep.* **2015**, *5*, 13616.
(34) Liu, Y.; Shaw, B.; Dickey, M. D.; Genzer, J. Sequential self-folding of polymer sheets. *Sci. Adv.* **2017**, *3*, No. e1602417.
(35) Hawkes, E.; An, B.; Benbernou, N. M.; Tanaka, H.; Kim, S.; Demaine, E. D.; Rus, D.; Wood, R. J. Programmable matter by folding. *Proc. Natl. Acad. Sci. U. S. A.* **2010**, *107*, 12441−12445.
(36) Laflin, K. E.; Morris, C. J.; Muqeem, T.; Gracias, D. H. Laser triggered sequential folding of microstructures. *Appl. Phys. Lett.* **2012**, *101*, 131901.
(37) Supekar, O. D.; Brown, J. J.; Eigenfeld, N. T.; Gertsch, J. C.; Bright, V. M. Atomic Layer Deposition Ultrathin Film Origami Using Focused Ion Beams. *Nanotechnology* **2016**, *27*, 49LT02.
(38) Si, K. J.; Sikdar, D.; Chen, Y.; Eftekhari, F.; Xu, Z.; Tang, Y.; Xiong, W.; Guo, P.; Zhang, S.; Lu, Y.; Bao, Q.; Zhu, W.; Premaratne, M.; Cheng, W. Giant plasmene nanosheets, nanoribbons, and origami. *ACS Nano* **2014**, *8*, 11086−11093.
(39) Mao, Y.; Pan, Y.; Zhang, W.; Zhu, R.; Xu, J.; Wu, W. Multi-direction-tunable three-dimensional meta-atoms for reversible switching between midwave and long-wave infrared regimes. *Nano Lett.* **2016**, *16*, 7025−7029.
(40) Liu, Z. Y.; Du, H.; Li, J.; Lu, L.; Li, Z.-Y.; Fang, N. X. Nano-kirigami with giant optical chirality. *Sci. Adv.* **2018**, *4*, No. eaat4436.

https://dx.doi.org/10.1021/acs.nanolett.0c01075
Nano Lett. 2020, 20, 4975−4984

(41) Murray, J.; Song, K.; Huebner, W.; O'Keefe, M. Electron beam induced crystallization of sputter deposited amorphous alumina thin films. *Mater. Lett.* **2012**, *74*, 12−15.
(42) Nakamura, R.; Ishimaru, M.; Yasuda, H.; Nakajima, H. Atomic rearrangements in amorphous Al2O3 under electron-beam irradiation. *J. Appl. Phys.* **2013**, *113*, 064312.
(43) Timoshenko, S. Analysis of bi-metal thermostats. *J. Opt. Soc. Am.* **1925**, *11*, 233−255.
(44) Cho, J. H.; James, T.; Gracias, D. H. Curving Nanostructures Using Extrinsic Stress. *Adv. Mater.* **2010**, *22*, 2320−2324.
(45) Miskin, M. Z.; Dorsey, K. J.; Bircan, B.; Han, Y.; Muller, D. A.; McEuen, P. L.; Cohen, I. Graphene-Based Bimorphs for Micron-Sized, Autonomous Origami Machines. *Proc. Natl. Acad. Sci. U. S. A.* **2018**, *115*, 466−470.
(46) Na, J. H.; Evans, A. A.; Bae, J.; Chiappelli, M. C.; Santangelo, C. D.; Lang, R. J.; Hull, T. C.; Hayward, R. C. Programming Reversibly Self-Folding Origami with Micropatterned Photo-Crosslinkable Polymer Trilayers. *Adv. Mater.* **2015**, *27*, 79−85.

https://dx.doi.org/10.1021/acs.nanolett.0c01075
Nano Lett. 2020, 20, 4975−4984